Izvestiya, Atmospheric and Oceanic Physics, Vol. 39, Suppl. 1, 2003, pp. S15–S26.

Validation of TOA Radiation and Clouds Simulated by Different Versions of the LMD General Circulation Model in Comparison to Satellite and Ground-Based Data[1]

A. V. Eliseev[1], H. Le Treut[2], I. I. Mokhov[1], M. Doutriaux-Boucher[3], and A. V. Chernokulsky[1, 4]

[1] *Obukhov Institute of Atmospheric Physics, Russian Academy of Sciences, Pyzhevskii per. 3, Moscow, 119017 Russia*
e-mail: eliseev@ifaran.ru, mokhov@ifaran.ru

[2] *Laboratoire de Meteorologie Dynamique du CNRS, Universite Pierre et Marie Curie, 4 place Jussieu, 752 Paris, cedex 05, France*

[3] *Laboratoire d'Optique Atmospherique, Universite des Sciences et Technologies de Lille, Villeneuve d'Ascq, France*

[4] *Lomonosov Moscow State University, Faculty of Geography, Vorob'evy gory, Moscow, 119992 Russia*

Received May 29, 2003

Abstract—The validation of cloudiness and radiative fluxes simulated by three versions of the Laboratoire de Meteorologie Dynamique (LMD) general circulation model (GCM) is performed against satellite and ground-based observations. These GCM versions include quite different cloud schemes and surface albedo representations. One model version implements the solar radiation diurnal cycle, while the others do not. Additionally, model versions are run with different spatial resolutions. Model validation is based on quite simple methodology to analyze the simulations for only three prechosen cross-sections in equatorial and middle latitudes, instead of studying the whole model field. It is shown that over middle latitudes simulated discrepancies exhibit a strong seasonal dependence. This is closely related to the representation of water vapor, cloudiness, and surface albedo in the model. In particular, errors in the simulated cloud radiative forcing (CRF) portray those for low-level cloudiness (for short-wave radiation) or high-level cloudiness (for long-wave radiation). As a whole, the errors in short-wave CRF are larger than those of the long-wave CRF, and are strongly amplified in summer. In the simulated total cloud amount, main errors are related to low-level cloudiness. It is also shown that the causes of the model deficiencies differ between versions. In some cases, errors coming from different origins could compensate each other. Although quite simple, the methodology followed in this intercomparison proved to be an effective approach for tracking systematic errors in a set of different model versions.

1. INTRODUCTION

Clouds constitute one of the most complex elements of the climate system, and the development of new parameterizations within current atmospheric general circulation models (GCMs) has had a strong impact on climate sensitivity experiments, such as in response to the CO_2 increase, for example.

The errors in cloud simulations may reflect problems in the specific cloud parameterizations, errors in the main fields simulated by the atmospheric model itself (including wind, moisture, and temperature), or errors in some of the specified parameters, such as surface albedo. Distinguishing among error sources constitutes the main objective of model validation through observed data. Comparison of different GCM simulations with observed data and analysis of cloudiness and radiation feedback operating in these simulations received a great deal of attention from meteorologists (see, e.g., [1–8]).

In recent years, the situation concerning the availability of data to validate cloudiness in climate models has changed drastically. The ISCCP time analysis extends from 1983 to the present, ERBE data have been made available to modelers and are followed by SCARAB and CERES data, SSMI has provided information about cloud water content, TOVS may provide information about the vertical profiles of temperature and water vapor, and Polder about the cloud thermodynamic phase (for review, see, e.g., [9]). New missions are expected in the future such as PICASSO/CENA, CLOUDSAT [9].

However, this growing amount of data still poses a very serious analysis problem. The choice of correct diagnostics to make comparisons between model and data or between different models is a crucial task.

In the present paper, we try to use combinations of different data (see Section 2) to diagnose the systematic errors in three versions of the LMD (Laboratoire de Meteorologie Dynamique du CNRS) general circulation model: LMD5, LMD5.2, and LMD6. These versions include quite different cloud schemes.

From LMD5 to LMD5.2 and LMD6, the parameters describing the precipitation processes and the interaction between clouds and radiation have been strongly modified. The scheme used in LMD5 corresponds to the scheme referred to as CO in [10]; the scheme used

[1] This article was submitted by the authors in English.

in LMD5.2 and LMD6 refers to MO. LMD6 includes new parameterization of convective processes in comparison to LMD5 and LMD5.2. In addition to this, surface processes were modified in the transition between LMD5 and LMD5.2, and LMD6 also includes the diurnal cycle, neglected in the preceding versions. The rest of the modules do not differ among the studied model versions. Further details are given in Section 3.

Comparing these three versions with observed data is a huge task, involving a large amount of diagnostics. We try to show in the present paper that the consideration of well-chosen longitudinal profiles is already a suitable diagnostics of many systematic errors.

In this paper, the three prechosen latitudinal belts are 50° N, 50° S, and the equatorial belt. The two former belts roughly correspond to the positions of midlatitudinal maxima in total cloudiness and permit one to diagnose midlatitude weather systems and storm tracks. The latter belt allows one to study tropical weather systems. Additionally, these cross-sections correspond to the key regions for validation of different parameterizations in a general circulation model. In particular, they are quite interesting for the purpose of the validation of cloudiness–radiation interactions because, generally, these are more significant at larger cloud amounts.

When analyzing only a limited amount of prechosen cross-sections instead of a whole map, one has to take care that the model considered does not shift climate structure along latitudinal and/or longitudinal belts. Otherwise, any conclusions about this model could be erroneous. This is not the case for the GCM versions considered here. Preliminary analysis has shown that all of them correctly reproduce positions of the main climatic structures, in particular, over the mentioned cross-sections. For cloud distributions, the corresponding plots are published in [11].

The subsequent analysis will be focused on the simulated radiative budget at the top of the atmosphere (TOA). First, a study of the GCM-simulated clear sky radiative fluxes will be performed because it is very useful before any analysis of the clouds and cloud impacts. Then, the comparison of radiative diagnostics and cloud diagnostics derived from ISCCP and ground-based data will be presented.

In this paper, several of the above diagnostics are presented in order to: (i) show that simple use of the available data can provide a very useful insight into the models, with potential implications for the analysis of large model experiments such as the Atmospheric Model Intercomparison Project (AMIP) or Coupled Model Intercomparison Project (CMIP), and (ii) to discuss some of the most common systematic errors found in the present generation of climate models.

Three versions of the LMD GCM are used here as a demonstration case to describe these systematic errors. While the description of the results below may sound somewhat negative, it is worth emphasizing that the overall performance of this GCM clearly demonstrates it is a state-of-the-art model (as it was in the AMIP intercomparison).

2. RADIATION AND CLOUD CLIMATOLOGIES

For the radiative fluxes at the top of the atmosphere, ERBE data [12, 13] are used. The estimated uncertainties in the monthly mean measured fluxes is about 6 W/m^2 for the short-wave component and 3 W/m^2 for the long-wave one [9]. While ERBE data exist since February 1985, only the data for December 1985–August 1988 are included in the present comparison. This is done in order to make composites for both June–July–August (JJA) and December–January–February (DJF) seasons, constructed from samples of the same length.

For cloudiness, two climatologies constructed in [14] are used. Two versions of the first climatology are constructed from the satellite ISCCP C2 and D2 data [15–17] for 1983–1988. The second climatology is based on ground-based observations [18, 19] over oceanic areas for 1930–1981 and over land areas for 1971–1981. Hereafter, these two climatologies are referred as C2, D2 and WEA, respectively. One must remember that C2 and D2 (corresponding to the observations from space) underestimate low- and mid-level cloudiness, while WEA (corresponding to observations the from ground) underestimates high- and mid-level cloud amount. Additionally, some problems concerning underreported low-level convective clouds in the WEA archive are noted by [20].

In the C2 and D2 climatology, clouds are stratified with respect to their observed heights. Clouds observed in the $680 < p < 1000$ hPa, $440 < p < 680$ hPa, $50 < p < 440$ hPa layers (where p stands for pressure) correspond to low-, mid-, and high-level clouds. In the WEA climatology, clouds are stratified with respect to their types. The cloud types Cu, St, Sc, and Cb are associated with low-level cloudiness; cloud types As, Ac, and Ns, with mid-level clouds; and cloud types Ci, Cc, and Cs, with high-level clouds.

An extensive comparison between C2 and WEA climatologies has been performed in [11, 14]. The new version of the ISCCP cloud climatology (version D2) uses a cloud retrieval algorithm different from that used for the older version C2 [17]. In [21], a single-year comparison between C2 and D2 was performed. It was shown that D2 depicts more low- and mid-level clouds over high latitudes and over deserts and more high-level clouds over continents. Analogous results have been obtained in [22] for zonal mean values averaged for 1983–1993.

3. DESCRIPTION OF GCM VERSIONS AND EXPERIMENTAL DESIGN

The various versions of the LMD GCM share the same finite difference numerics already described in the paper [23]. Over the years, the physical package of the models has been modified. We have chosen to compare here three versions: LMD5, LMD5.2, and LMD6, which have been extensively used for climate simulations, and also for intercomparison programs such as AMIP. They differ mostly by surface and cloud parameterizations.

3.1. LMD5

LMD5 [24] is the simplest of all versions. The surface scheme is a bucket model of 150 mm depth with no treatment of vegetation. The boundary layer is parameterized as a diffusion process over the lowest four layers of the model (out of a total of 11 layers). Exchange with the surface is also rather crudely parameterized, with a drag coefficient taking a fixed uniform value over both land and ocean and then modified by the stability dependence. The model contains a rather simple prognostic scheme for cloud water: condensed water precipitates when it exceeds 10^{-4} g/g (for water clouds) or 5% of the water vapor saturation value (for ice clouds). Clouds are considered to consist of ice or water depending on their cloud top temperature, higher or lower than –10°C. Finally, the diurnal cycle of the incoming solar radiation is not included.

Solar radiation is computed using the scheme described in [25]. Radiative fluxes are computed using a two-stream approximation, which accounts for the vertical profiles of temperature, water vapor, ozone, carbon dioxide, and clouds. Long-wave radiation is computed using the scheme CO described in [10].

In the intercomparison presented here, LMD5 was run with a horizontal resolution corresponding to 64 regularly spaced grid points in longitude and 50 grid points spaced regularly in sine of latitude, and with 11 vertical levels.

3.2. LMD5.2

LMD5.2 [26] represents an improvement with respect to LMD5 in several key aspects.

A representation of the vegetation is introduced: the SECHIBA model treats the evapotranspiration through the plants. Also, the albedo and surface roughness have been modified to take into account the heterogeneity resulting from vegetation.

The cloud model was also modified to avoid discontinuities in cloud water precipitation formulation. First, the separation between liquid and ice clouds was made depending on local temperature rather than cloud top temperature. A phase change is assumed to occur between 0 and –15°C with a fraction of ice clouds linearly increasing between these two values. The precipitation of liquid water q_e was done using the equation [27]

$$P_e = q_e C_t \left\{ 1 - \exp\left[-\left(\frac{q_e}{C_l} \right)^2 \right] \right\},$$

where q_e is the liquid cloud water content per unit area, $C_t = 5 \times 10^{-4}$ g/g, $C_l = 5 \times 10^{-4}$ s^{-1}. For ice clouds, the law corresponds to the sedimentation of ice crystals and is written as follows:

$$P_i = \frac{v q_i}{\Delta_z},$$

where Δ_z is vertical depth of a given layer, q_i is ice cloud content. Fall velocity of ice crystals is given by

$$v\,[\mathrm{ms}^{-1}] = 3.29(\rho_{\mathrm{air}} q_i)^{0.16},$$

where ρ_{air} (in kg/m^3) is air density.

Solar radiation is computed using the same scheme as for LMD5. In contrast, the long-wave radiation module changed in this model version to the scheme MO of [10].

In LMD5.2, cloud optical properties are simulated using the predicted liquid or ice water content depending on cloud type, but no diurnal cycle is used.

LMD5.2 was run with the horizontal resolution increased to 96×72 and with the number of vertical levels increased to 15. The latter induced a modified representation of the boundary layer with vertical diffusion formally imposed over the whole 15 layers, although it is significant in the few lower layers only.

3.3. LMD6

LMD6 [28] is similar to LMD5.2. But, unlike LMD5 and LMD5.2, the diurnal cycle is included. The cloud scheme has been slightly tuned. In this version, a new representation of microphysical processes was added by [29]. In the experiment considered here, the resolution is reduced to 64×50 (as it was for LMD5) in horizontal, with 11 levels in vertical. PBL diffusion is the same as for LMD5.

3.4. Numerical Experiments

Every model version has been integrated for 10 years, driven by the observed sea surface temperature for 1979–1988 [30]. These experiments closely correspond to those performed during the AMIP1 activity.

4. ANALYSIS OF MODEL SIMULATIONS

4.1. Clear-Sky Fluxes

The first step toward validation of the model simulated TOA radiative fluxes has to be an analysis of the corresponding clear-sky (CS) long-wave and short-

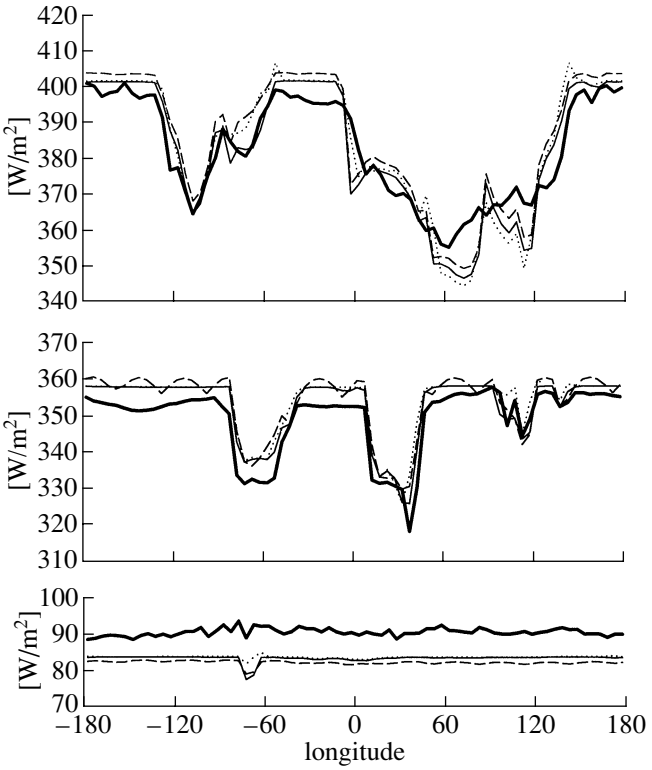

Fig. 1. JJA clear sky TOA short-wave radiative balance at 50° N (top), equator (middle), and 50° S (bottom). Curves are for the ERBE data (thick lines), LMD5 (thin solid lines), LMD5.2 (thin dotted lines), and LMD6 (thin dashed lines).

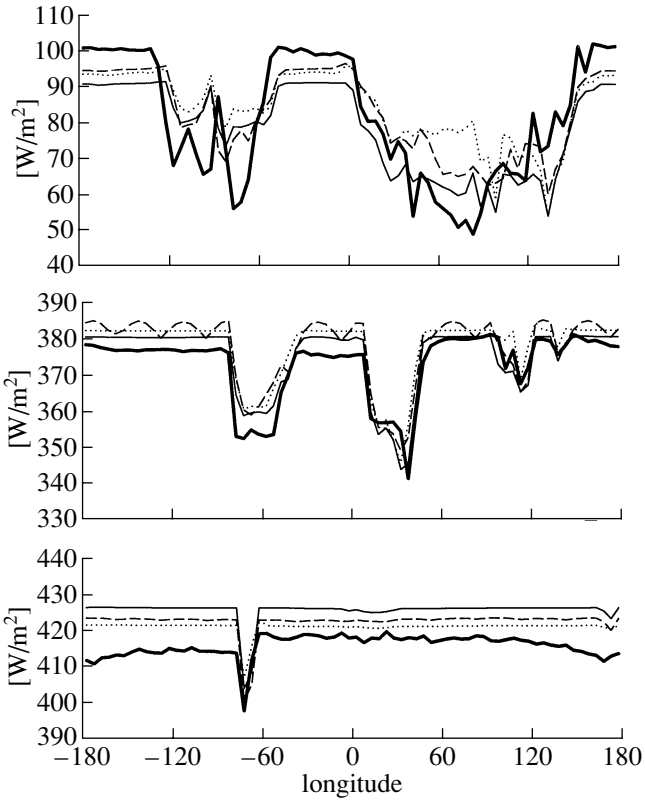

Fig. 2. DJF clear-sky TOA short-wave radiative balance. Panels and notations are the same as for Fig. 1.

wave fluxes to exclude the effect of clouds on radiative transfer and to concentrate on the effects of atmospheric water vapor, surface albedo description, and surface and atmospheric temperature performance. One has to emphasize that these effects are interrelated. In particular, the bias in the atmospheric temperature could bias the atmospheric water vapor content (either due to the biased evaporation or the dependence of saturated water vapor content on local temperature through the Clausius–Clapeyron equation). The bias in surface air temperature can additionally result in excessive or underestimated snow cover, which, in turn, affects ground albedo in the model. It could also affect atmospheric humidity via changes in the state of the land depending on local conditions (e.g., groundwater balance or permafrost characteristics). Additionally, surface and tropospheric air temperature are correlated through the lapse rate dependence on surface temperature [31, 32].

In the model, CS radiative fluxes were computed using method II of [1]. In general, this method samples grid cells which are wetter than those used in ERBE sampling. As a result, at the top of the atmosphere, the model simulates smaller clear sky outgoing long-wave and absorbed short-wave radiation than one obtains from the ERBE data. It was stated by [1] that simulated CS radiative fluxes differ between two methods only to a small degree (this conclusion was made analyzing the numerical experiments with the OSU/LLNL GCM), especially their SW component. Nevertheless, the latter assertion could be model dependent. In particular, [33], based on numerical experiments with the UCLA/GLA GCM, showed that even zonal mean differences between different methods of computation for clear-sky fluxes evaluation could be as large as 30 and 5–10 W/m^2 for short-wave and long-wave clear-sky fluxes, respectively.

Figure 1 shows the simulated CS TOA short-wave radiation (SWR) budget for the chosen latitudinal belts during the JJA season. Figure 2 presents the same plots, but for the DJF season. One can see the first systematic feature of the model: a strong seasonality of the albedo error in the GCM.

In winter, there is a clear overestimation of the planetary albedo over ocean with a clear underestimation in summer. These errors contribute to errors of the modeled CS short-wave fluxes of about 5–10 W/m^2 with the largest values reaching about 15 W/m^2 in the Pacific Ocean at 50° S during austral summer.

In particular, from the ERBE data, one can see that planetary albedo is significantly different over the Pacific and the Atlantic oceans. This difference cannot be attributed to different reflective states of the ocean:

according to the Surface Radiation Budget data (for December 1985–August 1988, the same period as for the ERBE data) [34, 35], the values of surface albedo over the two oceans are very similar to each other. It can be associated with the different water vapor contents over the Pacific and the Atlantic oceans. This possibility is checked using the NCEP reanalysis data of surface specific humidity [36]. In climatology, this variable is highly correlated with total water vapor content in a given atmospheric column due to the characteristic exponential profile of vapor distribution in the atmosphere. The latter analysis (not shown) exhibited that longitudinal variations of the planetary albedo in the ERBE data are to be associated with different water vapor amounts over the two oceans: more humid atmosphere implies smaller planetary albedo due to enhanced absorption. This feature evidently is not reproduced by the studied GCMs.

Over land, one also could note rather large discrepancies between observed and simulated TOA SWR over the equatorial cross-section (especially over America) and over winter midlatitudes where the difference between the observed and modeled CS TOA short-wave radiative budgets can be as large as 30 W/m^2. The latter errors may be due to snow representation. Additionally, rather strong discrepancies are found over Siberia during summer.

Figure 3 shows the plots of CS outgoing long-wave radiation (OLR) for the chosen latitudinal cross-sections for the JJA season. These cross-sections, as well as cross-sections for the DJF season (Fig. 4), again infer a strong seasonality in model bias for the CS OLR simulation and reflect model errors in simulating atmospheric water vapor content and surface and atmospheric temperatures. In particular, large errors are found for the equatorial belt and for summer northern midlatitudes. Over the equator (both for JJA and DJF) and over 50° N (during JJA), CS OLR is overestimated with typical deviation of 10 W/m^2 (maximum deviation is of about 30 W/m^2). The latter discrepancy occurs over equatorial America. All these errors are to be related to the errors in the representation of atmospheric water vapor. The model atmosphere is too dry and, therefore, emits too much clear-sky infrared radiation into space. Similarly remarkable underestimation of tropospheric precipitable water on both global and regional scales by the LMD GCM has been noted in the AMIP submitted experiment (performed with LMD5) by [37]. In contrast, northern midlatitudes during winter and southern midlatitudes during both winter and summer show rather good agreement between observed and simulated CS OLR with deviations not exceeding a few watts per square meter. The latter can also be related to the water vapor representation in the LMD GCM. The winter atmosphere is much drier than the summer one, and water vapor plays a less important role in the CS OLR computation. The comparison between the 50° N and 50° S cross-sections during

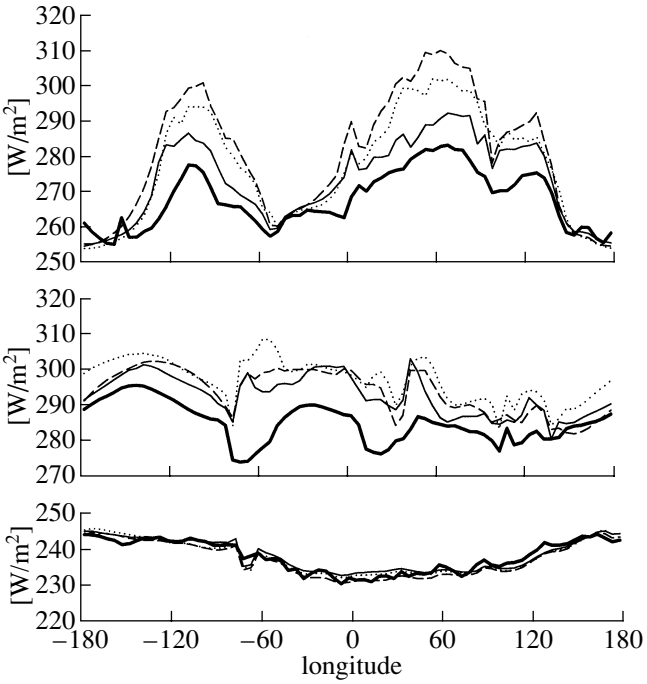

Fig. 3. JJA clear-sky TOA outgoing long-wave radiation. Panels and notations are the same as for Fig. 1.

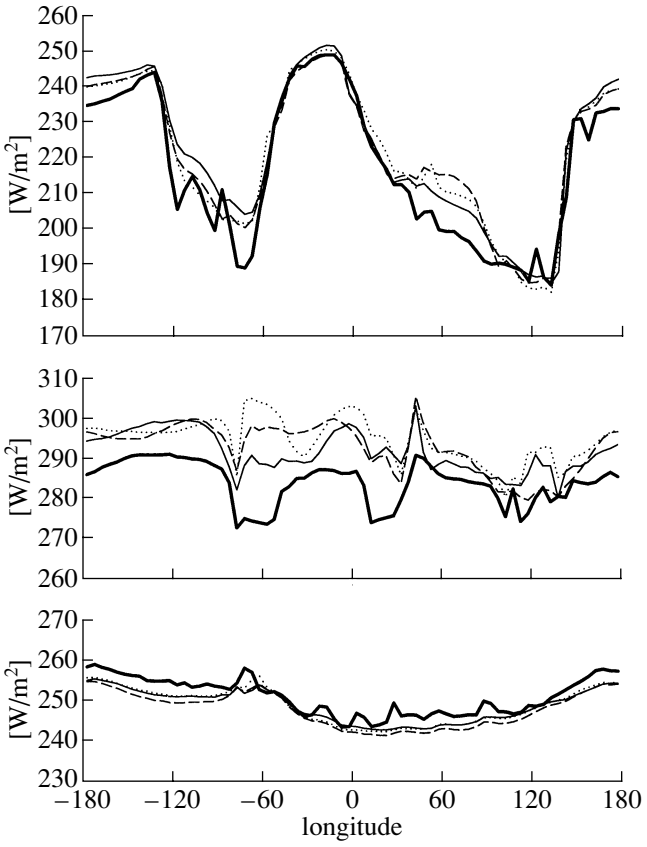

Fig. 4. DJF clear-sky TOA outgoing long-wave radiation. Panels and notations are the same as for Fig. 1.

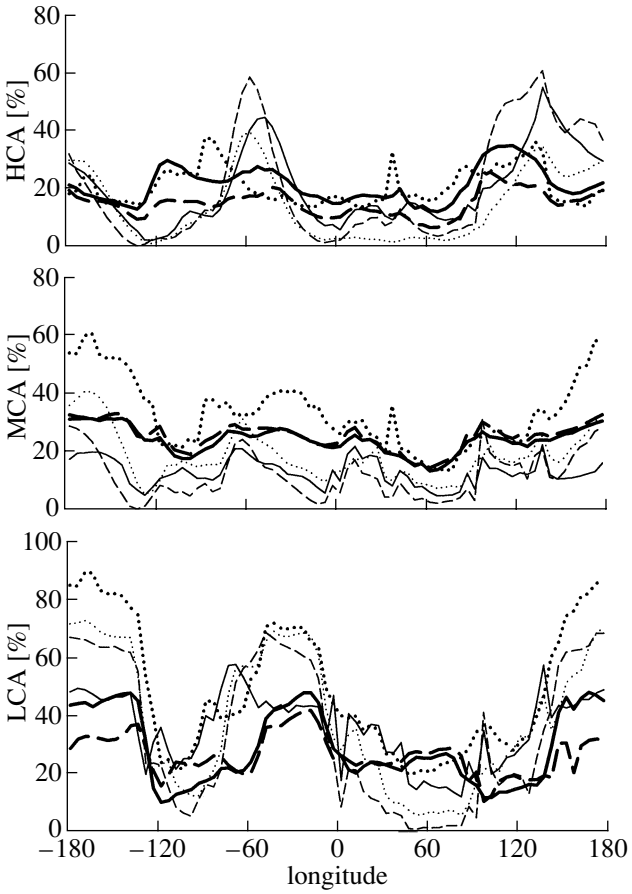

Fig. 5. JJA high- (top), mid- (middle), and low-level cloudiness (bottom) at 50° N. Curves are for the C2 data (thick solid lines), D2 data (thick long dashed lines), WEA data (thick dotted lines), LMD5 (thin solid lines), LMD5.2 (thin dotted lines), and LMD6 (thin dashed lines).

local summers suggests that the better agreement with the ERBE data found in the latter case is produced by the larger water vapor atmospheric content. The latter can be related to the larger percentage of the ocean in the southern compared to the northern midlatitudes.

One can also note that, for the CS OLR, LMD5 over land agrees unexpectedly better with observations than the other GCM versions. This may also be related to the simulated atmospheric moisture content, which is to be higher in LMD5 in comparison to the other studied versions. A possible cause for this is the implementation of the surface vegetation scheme into LMD5.2 and LMD6, which lowers atmospheric moisture content via suppressed evapotranspiration.

Errors in CS OLR and SWR fluxes are mutually compensated over ocean at the equator (during both JJA and DJF) and, at the summer, northern midlatitudes, resulting in rather good simulation of net CS radiation for these cases (not shown). In contrast, for the listed cross-sections over land, errors in the clear-sky short-wave and long-wave fluxes are not compensated, and clear-sky net radiation deviates from the ERBE data by up to 20 W/m^2. For the southern midlatitudes (during both seasons), CS net radiation is well represented over land for all three model versions but deviates strongly over oceans. The latter deviations can be as large as 15 W/m^2 during the austral summer over the Atlantic Ocean with smaller values over the Pacific Ocean and even up to 30 W/m^2 during the austral winter, with similar values for both southern oceans.

4.2. Cloudiness

In the subsequent analysis, clouds are stratified in accordance with simulated heights. Namely, for the coarse-resolution simulations (LMD5 and LMD6), clouds located at the GCM vertical levels 1–4, 5–7, and 8–11 are treated as low-, mid-, and high-level clouds [38], respectively. These model levels correspond roughly to the layers $780 < p < 1000$ hPa, $380 < p < 780$ hPa, and $15 < p < 380$ hPa, respectively. For the high-resolution simulations (LMD5.2), the low-, mid-, and high-level clouds are considered to belong to the GCM levels 1–6, 7–10, and 11–15, respectively (or to the layers $700 < p < 1000$ hPa, $280 < p < 700$ hPa, and $10 < p < 280$ hPa, respectively) (Doutriaux-Boucher, 1997). One could note that both the coarse- and high-resolution cloud stratifications differ from that used for both observed climatologies (see Section 2).

Total cloud amount (TCA) is evaluated assuming random overlap of clouds in the layers mentioned above. Unlike LMD5 and LMD5.2, LMD6 includes the solar radiation diurnal cycle. This leads to differences in the details of the computation of monthly mean TCA between model versions. For both LMD5 and LMD5.2, total cloud amount has been determined on the basis of instantaneous model output. The monthly mean TCA has then been computed using these instantaneous TCA. For LMD6, instantaneous GCM output has been averaged daily to give a daily mean (three-dimensional) cloudiness. The latter has been used to compute a daily mean TCA, which, in turn, has been averaged to give a monthly mean total cloud amount. The difference between these approaches could itself affect the results of comparison. In [38], using the experiments with LMD6, it was shown that, in the latter case, overall TCA is generally increased, as well as its longitudinal contrast.

In general, C2 and D2 observe less low- and mid-level clouds during both seasons than WEA (see Fig. 5 as an example). The deviations between these ground- and satellite-based climatologies are especially large for low-level cloud amounts (up to 40%). For high-level clouds, agreement between them is better, with few exceptions.

Simulated cloudiness shows a seasonality of error when compared to the observed data. In particular, total cloud amount is generally underestimated for summer midlatitudes (see Fig. 6 as an example). This underestimation comes from the corresponding underestimation

of low- and mid-level cloud amounts (LCA and MCA, respectively) (Fig. 5). Similar TCA underestimation originating from too small LCA over summer midlatitude oceans has also been found for ECHAM4 [39]. High-level cloud amount (HCA) is strongly overestimated over ocean for 50° S and over land for 50° N, and underestimated over ocean for the latter belt (Fig. 5).

During winter (not shown), midlatitudinal cloudiness is generally overestimated. For low-level cloudiness, it occurs mainly over land at 50° N, irrespective of the chosen climatology. In turn, MCA and HCA are higher than those observed for both 50° N and 50° S cross-sections. For the former belt, MCA, if compared to C2 and WEA, is overestimated for both ocean and land longitudes; HCA is overestimated only over oceans. Both discrepancies are greatly reduced if compared to the D2 dataset, especially over Eurasia. For the latter cross-section, if compared to the C2 and WEA data, HCA is higher than that observed everywhere, but MCA is overestimated only over oceans (surprisingly, LMD5 simulates MCA better than the other model versions). If compared to D2, MCA is also overpredicted over the oceans, but the agreement of the modeled and observed HCA is improved over eastern Eurasia. Nevertheless, main errors in the simulations of TCA are associated with LCA. This is true irrespective of the chosen observed climatology. In particular, TCA over winter northern midlatitudes is overestimated over continents with similar errors in the simulated LCA. For the southern midlatitudes, TCA agrees with the observed data reasonably well (in spite of the above-mentioned deviations in MCA and HCA) due to well-simulated low-level cloudiness.

Over the equator, cloudiness shows much less difference between the two seasons. Similar qualitative characteristics of the simulated cloudiness could be traced for both JJA and DJF composites. In particular, irrespective of the chosen cloud climatology, TCA is overestimated over the Pacific Ocean with smaller deviations from the observed data over other longitudes (Fig. 6). This error comes mainly from the simulated LCA and, to a smaller extent, from the high-level cloudiness (with the agreement with D2, respect to the C2 and WEA data). Mid-level cloudiness falls into the range of observed climatologies (C2 and WEA) and does not contribute to the discrepancies of the simulated TCA (at least within the limits of the present analysis).

Simulated total cloud amount also differs between model versions. One can note, however, that its cross-sections resemble each other for LMD5.2 and LMD6 and (in general) strongly deviate from those for LMD5. The latter leaves out the possibility that the TCA differences between versions could be explained as a result of different approaches of its evaluation (see above). In contrast, they could be traced to the formulations of different GCM versions.

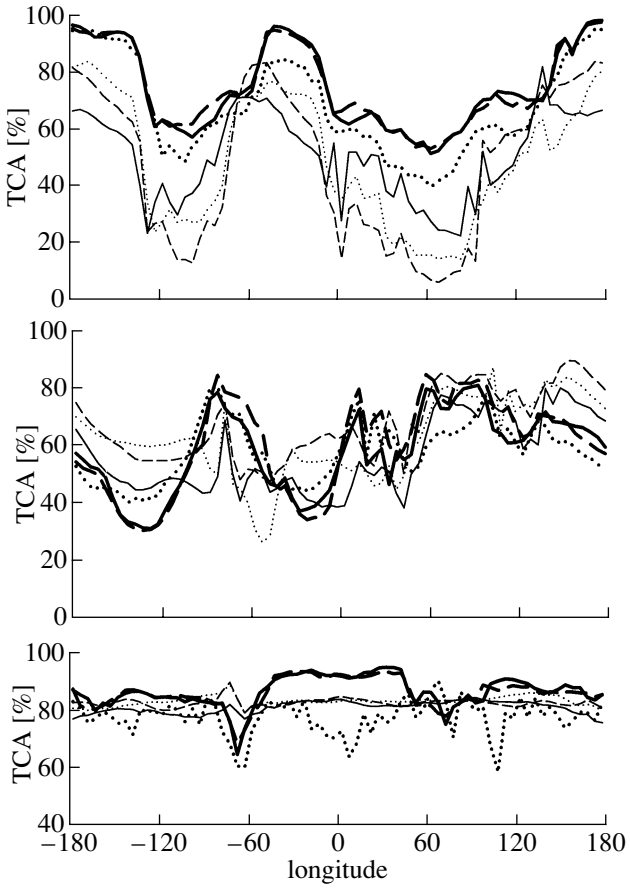

Fig. 6. JJA total cloud amount (%) at 50° N (top), equator (middle), and 50° S (bottom). Notations are the same as for Fig. 5.

4.3. Total Sky Fluxes and Cloud Radiative Forcing

For the model, as well as for the ERBE data, the CRF is defined as a difference between corresponding all sky and clear sky TOA fluxes [40, 41]. It has to be noted that this definition of the short-wave (SW) CRF differs from that used by [3, 42], where the term $(\bar{\alpha}_c - \bar{\alpha})\Delta S$ has been extracted from the total SW CRF to account only for seasonal cloudiness variability (where $\bar{\alpha}_c$ and $\bar{\alpha}$ are the annual mean clear and all sky planetary albedos, respectively, and ΔS is the seasonal variation of TOA incoming solar energy). The aim of the present study is to diagnose the GCM in terms of its cloud and radiative seasonal mean fields, and not to study the seasonal variations of SW CRF itself. Therefore, this term is retained in the definition of short-wave cloud radiative forcing.

It has to be noted that differences in the formulation of clear sky fluxes from the ERBE data and the GCM (Section 4.1) have also to bias the simulated CRF with the same magnitude, as it was for clear sky radiation.

In general, as well as the fields studied above, all sky radiation and CRF show strong seasonality in their

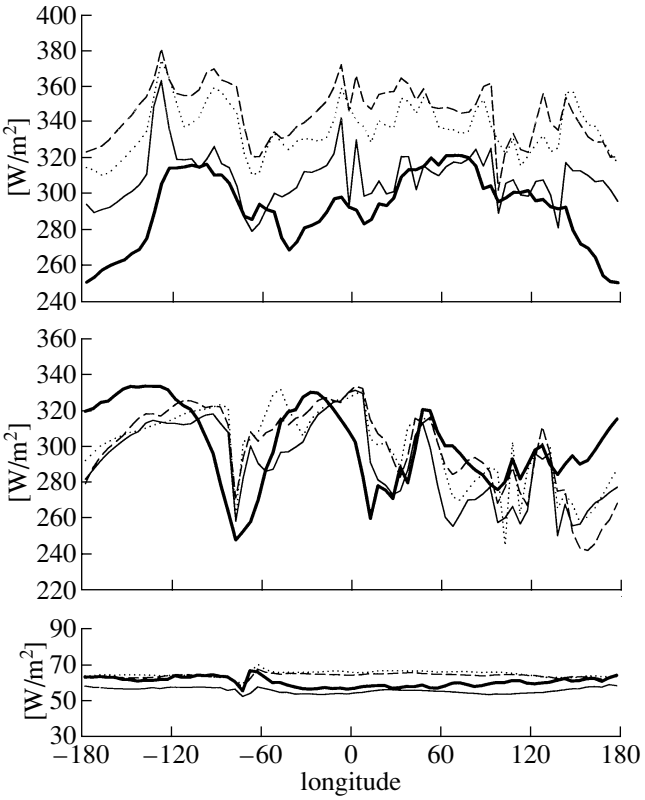

Fig. 7. JJA all sky TOA short-wave radiative balance. Panels and notations are the same as for Fig. 1.

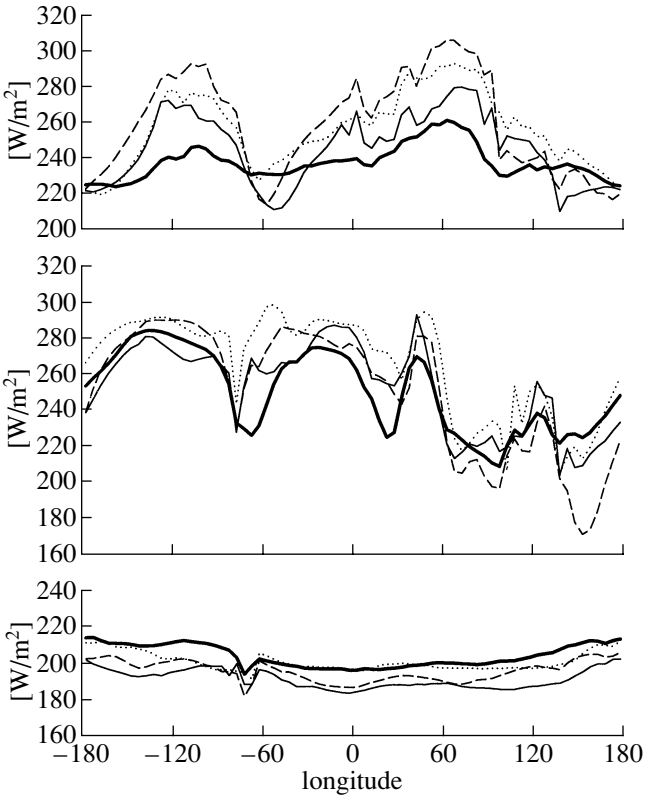

Fig. 8. JJA all sky outgoing long-wave radiation. Panels and notations are the same as for Fig. 1.

errors with respect to the ERBE data: for both short-wave and long-wave components, as well as for net radiation, the deviations are amplified in summer and much reduced in winter (Figs. 7–10).

4.3.1. Summer midlatitudes. For summer midlatitudes, models strongly (with errors up to 70 W/m^2 in the Northern Hemisphere) overestimate all sky short-wave radiative heating (Fig. 7). These errors are much more pronounced than those in the corresponding CS fluxes and mainly related to the errors in the short-wave CRF (Figs. 9, 10). The latter, being negative by sign, is smaller by magnitude than that derived from observations. It was shown in [43] that, in the LMD GCM, low-level clouds contribute basically to the simulated value of SW CRF. Taking this in mind, the underestimated SW CRF is in agreement with the underestimated summer midlatitude LCA (see Section 4.2 for details). Of course, this does not exclude that higher-level clouds also playing a significant role in the simulated value of SW CRF.

In contrast, the long-wave part of cloud radiative forcing (LW CRF) over the summer midlatitudes shows more complex behavior. For the 50° N belt, during boreal summer, all sky OLR is overestimated almost everywhere, except in a narrow area near the eastern coast of North America (Fig. 8) where it is underestimated. Errors in the simulated OLR came from two additive sources: both CS OLR and LW CRF comparably contribute to all the sky OLR errors. The area near the North American coast (about 60° W) mentioned above with the smaller than observed OLR is due solely to the CRF effect. Longitudinal dependence of the simulated long-wave CRF bears much resemblance to that of the HCA (Fig. 5). It is again in agreement with the results of [43], where it was found that, in the LMD GCM, LW CRF is mainly affected by high-level clouds. This feature is also exhibited in other models [3, 33, 44].

For the 50° S cross-section during austral summer, OLR is underestimated (with discrepancies up to 25 W/m^2) due to errors in the simulated LW CRF. As for the northern midlatitudes, errors come both from the clear-sky and cloudy fluxes with a longitudinal dependence similar to that exhibited by HCA.

Over summer northern midlatitudes, net radiation is overestimated, and errors are rather large (up to 80 W/m^2 over the Pacific Ocean, 60 W/m^2 over Atlantic Ocean, and about 20 W/m^2 over land). It is interesting to note that errors in the CS part of the net radiative balance are almost compensated everywhere in the northern summer midlatitudes except Eurasia (see Section 4.1). As a result, discrepancies in the simulated net radiation are basically due to cloudy fluxes. Overestimation of all sky net radiation is exhibited also for the 50° S belt, but,

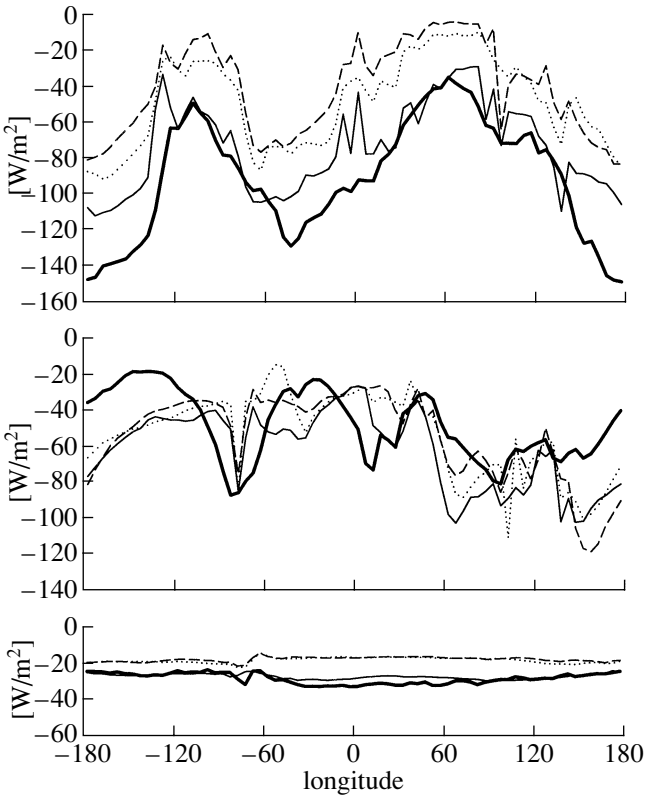

Fig. 9. JJA TOA short-wave CRF. Panels and notations are the same as for Fig. 1.

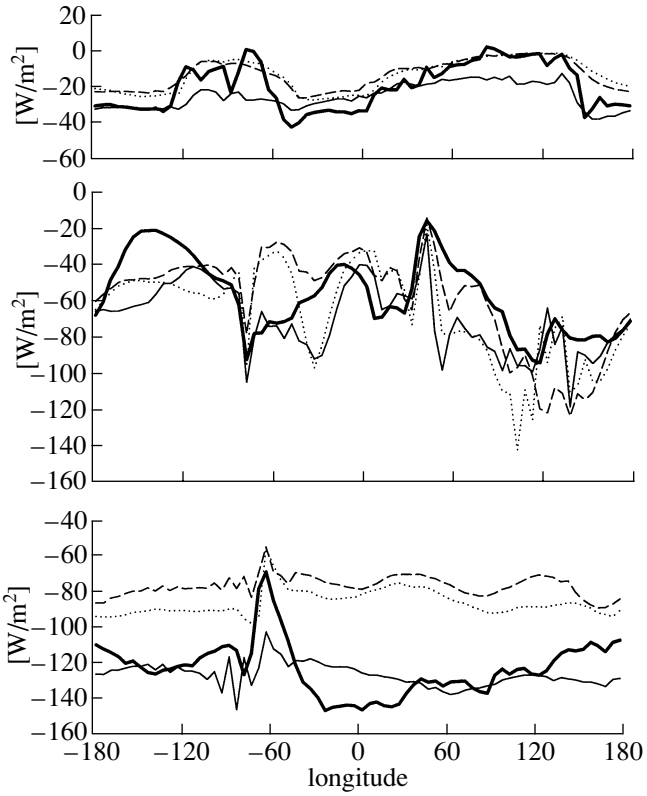

Fig. 10. DJF TOA short-wave CRF. Panels and notations are the same as for Fig. 1.

in the latter case, the errors in SWR and OLR have different signs. Also, in this case, both CS and cloudy fluxes contribute comparably to the deviations of the simulated TOA net radiation.

4.3.2. Winter midlatitudes. For winter midlatitudes, the errors are much reduced. All sky TOA short-wave radiative balance is very close to observations. For 50° S during JJA, errors are not higher than a few W/m^2; for 50° N during DJF they could be larger—about 25 W/m^2 at most longitudes. In all cases, LMD5 underestimates all sky SWR, while LMD5.2 and LMD6 overestimate it. Such differences among model versions come from SW CRF. In particular, over land, LMD5.2 and LMD6 adequately reproduce SW CRF and LMD5 simulates higher than observed magnitude of short-wave cloud radiative forcing. Over ocean, the situation is reversed: LMD5 agrees well with observations, and LMD5.2 and LMD6 underestimate the magnitude of SW CRF (Figs. 9, 10).

In Section 4.1, q_e it was shown that CS OLR is well simulated for winter midlatitudes. As a result, all deficiencies in the simulated OLR are originating from its cloudy part. For both midlatitudinal cross-sections, LW CRF is higher and all sky OLR is smaller than those observed with errors up to 20 W/m^2. As it was for summer, the longitudinal dependence of the deviations of the simulated LW CRF from the ERBE data mainly portrays respective deviations of HCA from the observed climatologies.

Winter TOA net radiation for midlatitudinal cross-sections shows that all model versions underestimate winter radiative cooling of the Earth–atmosphere system (the only overestimation is found for Siberia). The deviations could be as large as 15 W/m^2. For the northern midlatitudes, a compensation between overestimated CS net cooling (over ocean) and too small net CRF takes place. For the latter case, the simulations deviate from the observations with typical values of 40 W/m^2 with the largest deviation of 60 W/m^2 in the Pacific Ocean. This compensation does not occur over northern midlatitude land, or over southern midlatitudes. For both latter cases, errors in CS net radiation and net CRF have the same sign.

As a whole, for both seasons, largest errors in the simulated net CRF came from its short-wave part. It has to be noted, however, that the large amplification SW CRF from summer to winter is mainly due to the corresponding difference of TOA incoming solar radiation between these two seasons. In particular, characteristic differences between the modeled SW CRF and that observed increases about fivefold from winter to summer at 50° latitude. It can be compared to the corresponding fivefold increase of SW CRF for midlatitudinal cross-sections. On the other hand, it emphasizes

that cloudiness–short-wave radiation interaction plays a more important role in summer than in winter with a respective larger contribution to the net radiative budget.

4.3.3. Equatorial belt. Over the equator, deficiencies in the simulated absorbed TOA short-wave radiation are mainly due to the respective errors in the simulated SW CRF (Figs. 7, 9, 10). These errors portray the errors in simulated cloudiness (especially over the Pacific Ocean; see Section 4.2).

5. DISCUSSION AND CONCLUSIONS

In this paper, an analysis of clouds and TOA radiative fluxes simulated by three versions of the LMD GCM against ground- and satellite-based data is presented.

The GCM versions under study (LMD5, LMD5.2, and LMD6) include quite different cloud schemes and surface albedo representation, due to the inclusion of vegetation effects in the latter two versions. Unlike LMD5 and LMD5.2, LMD6 implements the diurnal cycle of the incoming solar radiation. Additionally, LMD5.2 is run with increased horizontal and vertical spatial resolution.

The presented intercomparison is limited only to the three prechosen latitudinal belts to diagnose equatorial and midlatitudinal weather systems. In particular, simulated clear-sky short-wave radiative fluxes show strong seasonality in their errors. For clear-sky short-wave radiative fluxes, better performance is noted for the versions with an implemented vegetation scheme (especially for LMD5.2). Some remaining errors could be traced to the deficiencies in the simulated snowcover affecting surface albedo over midlatitudinal continents during winter. Errors in the modeled clear sky OLR lead one to the conclusion that either the model atmosphere is too dry over summer northern midlatitudes or the latter are overheated.

Strong errors are associated with the simulated cloud radiative forcing. Such errors in short-wave and long-wave parts of CRF portray those in the simulated low- and high-level cloud amounts, respectively. This is in accordance with the findings of [43] and [33], using the LMD GCM and the UCLA/GLA GCM, respectively. Similar interrelations between high-level cloudiness and long-wave CRF has also been found in [44] and in [3], using an analysis with the CCM2 GCM and with a large ensemble of GCMs, respectively. The association between the deficiencies in the simulated LCA and SW CRF is in contrast with the latter study where it was shown that clouds from all levels contribute significantly to the short-wave cloud radiative forcing. It is interesting to note that an intermediate situation has been noted for the CCM2 GCM, where SW CRF depend mainly on low- and mid-level cloud amounts without any significant contribution from high-level cloudiness [44].

In particular, strong errors in both the simulated low- and high-level cloudiness are found over the equatorial Pacific Ocean for both seasons. These errors persist for all GCM versions, raising a question concerning the model convection scheme. Usually, different convective algorithms differ in the intensity of the vertical moisture transport (e.g., [44–47]). In such a case, one could expect that errors in the simulated HCA and LCA are to be of different signs. Some hint for this is provided by the fact that the studied GCM versions overestimate the low-level cloud amount more strongly than the high-level one: convection in the LMD GCM could be weaker than in the real world. Nevertheless, this is (if true) overcompensated by the too moist atmosphere in the equatorial Pacific Ocean, resulting in general overestimation of both LCA and HCA there.

Overestimated low-level cloud amounts (both over the equator and over the midlatitudes) could also be due to the specification of the model planetary boundary layer (PBL) parameterization. In particular, it was found in [5] that, in general, GCMs tend to confine water vapor inside the lower troposphere, due to their PBL formulation. This could obviously result in overpredicted low-level cloudiness.

Most state-of-the-art GCMs show an excessive heating of the Southern Hemisphere ocean [48]. This systematic error is reflected in the coupled models, as was shown by the recent CMIP intercomparison [49]. The three versions of the LMD GCM make no exception to this rule. But the origin of this bias may vary from version to version:

In all cases, there is a clear-sky contribution as is shown above.

The SW CRF may be underpredicted, but it is not true for all the three model versions. LMD5 (probably because it retains more ice cloud water until the latter precipitates) tends to better simulate this feature.

The LW CRF is overpredicted.

In general, although quite simple, the methodology followed here proved to be an effective approach of systematic errors in a set of different versions of models, and gives useful insights into the deficiencies in the GCM physical parameterizations. In particular, it could be useful in future model intercomparison, such as the later stages of AMIP, yielding a simple but meaningful way to compare the models' performance.

ACKNOWLEDGMENTS

The authors wish to thank V.M. Kattsov for discussions during the preparation of this paper.

The paper was supported by the Joint Agreement Program between the Centre National de la Recherche Scientifique and the Russian Academy of Sciences and partly by the Russian Ministry for Industry, Science, and Technology (contract no. 43.016.11.1616), Russian Foundation for Basic Research (grant no. 02-05-64573), and the Russian Program for Supporting the Leading Scientific Schools (grant no. 1636.2003.5).

REFERENCES

1. Cess, R.D. and Potter, G.L., Exploratory Studies of Cloud Radiative Forcing with a General Circulation Model, *Tellus*, 1987, vol. 39a, pp. 460–473.
2. Cess, R.D., Potter, G.L., Blanchet, J.P., Boer, G.J., Del Genio, A.D., Deque, M., Dymnikov, V., Galin, V., Gates, W.L., Ghan, S.J., Kiehl, J.T., Lacis, A.A., Le Treut, H., Li, Z.-X., Liang, X.-Z., McAvaney, B.J., Meleshko, V.P., Mitchell, J.F.B., Morcrette, J.-J., Randall, D.A., Rikus, L., Roeckner, E., Royer, J.F., Schlese, U., Sheinin, D.A., Slingo, A., Sokolov, A.P., Taylor, K.E., Washington, W.M., Wetherald, R.T., Yagai, I., and Zhang, M.-H., Intercomparison and Interpretation of Climate Feedback Processes in 19 Atmospheric General Circulation Models, *J. Geophys. Res.*, 1990, vol. 95, pp. 16601–16615.
3. Cess, R.D., Zhang, M.H., Potter, G.L., Alekseev, V., Barker, H.W., Bony, S., Dazlich, D.A., Del Genio, A.D., Deque, M., Dix, M.R., Dymnikov, V., Esch, M., Fowler, L.D., Fraser, J.R., Galin, V., Gates, W.L., Hack, J.J., Ingram, W.J., Kiehl, J.T., Kim, Y., Le Treut, H., Liang, X.-Z., McAvaney, B.J., Meleshko, V.P., Morcrette, J.-J., Randall, D.A., Roeckner, E., Schlesinger, M.E., Sporyshev, P.V., Taylor, K.E., Timbal, B., Volodin, E.M., Wang, W., Wang, W.C., and Wetherald, R.T., Comparison of Seasonal Change in Cloud–Radiative Forcing from Atmospheric General Circulation Models and Satellite Observations, *J. Geophys. Res.*, 1997, vol. 102, pp. 16593–16603.
4. Gates, W.L., The Atmospheric Model Intercomparison Project (AMIP), *Bull. Am. Meteorol. Soc.*, 1992, vol. 73, pp. 1962–1970.
5. Randall, D.A., Cess, R.D., Blanchet, J.P., Boer, G.J., Dazlich, D.A., Del Genio, A.D., Deque, M., Dymnikov, V., Galin, V., Ghan, S.J., Lacis, A., Le Treut, H., Li, Z.-X., Liang, X.-Z., McAvaney, B.J., Meleshko, V.P., Mitchell, J.F.B., Morcrette, J.-J., Potter, G.L., Rikus, L., Roeckner, E., Royer, J.F., Schlese, U., Sheinin, D.A., Slingo, J., Sokolov, A.P., Taylor, K.E., Washington, W.M., Wetherald, R.T., Yagai, I., and Zhang, M.-H., Intercomparison and Interpretation of Surface Energy Fluxes in Atmospheric General Circulation Models, *J. Geophys. Res.*, 1992, vol. 97, pp. 3711–3724.
6. Randall, D.A., Cess, R.D., Blanchet, J.P., Chalita, S., Colman, R., Dazlich, D.A., Del Genio, A.D., Keup, E., Lacis, A., Le Treut, H., Liang, X.-Z., McAvaney, B.J., Mahfouf, J.F., Meleshko, V.P., Morcrette, J.-J., Norris, P.M., Potter, G.L., Rikus, L., Roeckner, E., Royer, J.F., Schlese, U., Sheinin, D.A., Sokolov, A.P., Taylor, K.E., Wetherald, R.T., Yagai, I., and Zhang, M.-H., Analysis of Snow Feedbacks in 14 General Circulation Models, *J. Geophys. Res.*, 1994, vol. 99, pp. 20757–20771.
7. Mokhov, I.I., Galin, V.Y., Degtyarev, A.I., Kruglova, E.N., Meleshko, V.P., Sokolov, A.P., Sporyshev, P.V., Stenchikov, G.L., Trosnikov, I.V., and Sheinin, D.A., Comparison of General Circulation Models: Diagnostics of Intraannual Evolution of Cloudiness, *Izv., Atmos. Ocean. Phys.*, 1994, vol. 30, pp. 497–512.
8. Weare, B.C., Mokhov, I.I., and AMIP Modeling Groups, Evaluation of Total Cloudiness and Its Variability in the Atmospheric Model Intercomparison Project, *J. Climate*, 1995, vol. 8, pp. 2224–2238.
9. Wielicki, B.A., Cess, R.D., King, M.D., Randall, D.A., and Harrison, E.F., Mission to Planet Earth: Role of Clouds and Radiation in Climate, *Bull. Am. Meteorol. Soc.*, 1995, vol. 76, pp. 2125–2153.
10. Le Treut, H., Li, Z.X., and Forichon, M., Sensitivity of the LMD General Circulation Model to Greenhouse Forcing Associated with Two Different Cloud Water Parameterizations, *J. Climate*, 1994, vol. 7, pp. 1827–1841.
11. Doutriaux, M., Le Treut, H., and Seze, G., Une etude de la couverture nuagese: Comparaison des climatologies issues de l'observation satellitaire des observations au sol et de modeles de circulation generale du LMD, *Note Interne du LMD no. 196*, Paris: Laboratoire de Meteorologie Dynamique du CNRS, 1995.
12. Barkstrom, B.R., The Earth Radiation Budget Experiment (ERBE), *Bull. Am. Meteorol. Soc.*, 1984, vol. 65, pp. 1170–1185.
13. Barkstrom, B.R. and Smith, G.L., The Earth Radiation Budget Experiment: Science and Implementation, *Rev. Geophys.*, 1986, vol. 24, pp. 379–390.
14. Mokhov, I.I. and Schlesinger, M.E., Analysis of Global Cloudiness: 2. Comparison of Ground-Based and Satellite-Based Cloud Climatologies, *J. Geophys. Res.*, 1994, vol. 99, pp. 17045–17065.
15. Schiffer, R.A. and Rossow, W.B., The International Satellite Cloud Climatology Project (ISCCP): The First Project of the World Climate Research Program, *Bull. Am. Meteorol. Soc.*, 1983, vol. 64, pp. 779–784.
16. Rossow, W.B. and Schiffer, R.A., ISCCP Cloud Data Products, *Bull. Am. Meteorol. Soc.*, 1991, vol. 72, pp. 2–20.
17. Rossow, W.B. and Schiffer, R.A., Advances in Understanding Clouds from ISCCP, *Bull. Am. Meteorol. Soc.*, 1999, vol. 80, pp. 2261–2287.
18. Warren, S.G., Hanh, C.J., London, J., Chervin, R.A., and Jenne, R., Global Distribution of Total Cloud Cover and Cloud Type Amounts over Land, *NCAR Tech. Note no. TN-273 + STR National Center for Atmospheric Research Boulder CO*, 1986.
19. Warren, S.G., Hanh, C.J., London, J., Chervin, R.A., and Jenne, R., Global Distribution of Total Cloud Cover and Cloud Type Amounts over Ocean, *NCAR Tech. Note no. TN-317 + STR National Center for Atmospheric Research Boulder CO*, 1988.
20. Sun, B., Groisman, P.Ya., and Mokhov, I.I., Recent Changes in Cloud-Type Frequency and Inferred Increases in Convection over the United States and the Former USSR, *J. Climate*, 2001, vol. 14, pp. 1864–1880.
21. Doutriaux-Boucher, M. and Seze, G., Significant Changes between the ISCCP C and D Cloud Climatologies, *Geophys. Res. Lett.*, 1998, vol. 25, pp. 4193–4196.
22. Hatzianastassiou, N., Cleridou, N., and Vardavas, I.M., Global Radiation Budget Using the New ISCCP D2 Satellite Data, *IRS 2000: Current Problems in Atmospheric Radiation*, Smith, W.L. and Timofeyev, Yu.M., Eds., Hampton, Virginia: A. Deepak Publ., 2001, pp. 524–527.
23. Sadourny, R. and Laval, K., January and July Performance of the LMD General Circulation Model, *New Perspectives in Climate Modeling*, Berger, A. and Nicolis, C., Eds., Amsterdam: Elsevier, 1984, pp. 173–198.

24. Polcher, J., Harzallah, A., Bony, S., Chalita, S.N., Cohen-Solal, E., Forichon, M., Hourdin, F., Le Treut, H., Levan, P., Li, Z.-X., and Rogel, P., Le cycle 5 du modele de circulation generale du LMD, *Note Interne du LMD no. 170*, Paris: Laboratoire de Meteorologie Dynamique du CNRS, 1991.
25. Fouquart, Y. and Bonnel, B., Computation of Solar Heating of the Earth's Atmosphere: A New Parameterization, *Beitr. Phys. Atmos.*, 1980, vol. 53, pp. 35–62.
26. Forichon, M., Tests sur le cycle LMD5bis du modele de circulation generale du LMD, *Note Interne du LMD no. 190*, Paris: Laboratoire de Meteorologie Dynamique du CNRS, 1994.
27. Sundquist, H., A Parameterization Scheme for Nonconvective Condensation Including Prediction of Cloud Water Content, *Q. J. Roy. Meteorol. Soc.*, 1978, vol. 104, pp. 677–690.
28. Polcher, J. and Laval, K., A Statistical Study of the Regional Impact of Deforestation on Climate in the LMD GCM, *Clim. Dyn.*, 1994, vol. 10, pp. 205–219.
29. Boucher, O., Le Treut, H., and Baker, M.B., Precipitation and Radiation Modeling in a General Circulation Model: Introduction of Cloud Microphysical Processes, *J. Geophys. Res.*, 1995, vol. 100, pp. 16395–16414.
30. Reynolds, R.W., A Real-Time Global Sea Surface Temperature Analysis, *J. Climate*, 1988, vol. 8, pp. 75–86.
31. Gulev, S.K., Zveryayev, I.I., and Mokhov, I.I., Tropospheric Lapse Rate as a Function of Surface Temperature Conditions, *Izv., Atmos. Ocean. Phys.*, 1991, vol. 27, pp. 287–294.
32. Mokhov, I.I., *Diagnostics of the Climate System Structure*, St. Petersburg: Gidrometeoizdat, 1993.
33. Harshvardhan, Randall, D.A., Corsetti, T.G., and Dazlich, D.A., Earth Radiation Budget and Cloudiness Simulations with a General Circulation Model, *J. Atmos. Sci.*, 1989, vol. 46, pp. 1922–1942.
34. Laszlo, I. and Pinker, R.T., Impact of Changes to Water Vapor Parameterization on Surface Short-Wave Radiative Fluxes, *Current Problems in Atmospheric Radiation*, Smith, W., Ed., Hampton, Virginia: A. Deepak Publ., 1997, pp. 526–529.
35. Laszlo, I., Pinker, R.T., and Whitlock, C.H., Comparison of Short-Wave Fluxes Derived from Two Versions of the ISCCP Products, *Current Problems in Atmospheric Radiation*, Smith, W., Ed., Hampton, Virginia: A. Deepak Publ., 1997, pp. 762–765.
36. Kalnay, E., Kanamitsu, M., Kistler, R., Collins, W., Deaven, D., Gandin, L., Iredell, M., Saha, S., White, G., Woollen, J., Zhu, Y., Leetmaa, A., Reynolds, R., Chelliah, M., Ebisuzaki, W., Higgins, W., Janowiak, J., Mo, K.C., Ropelewski, C., Wang, J., Jenne, R., and Joseph, D., The NCEP/NCAR 40-Year Reanalysis Project, *Bull. Am. Meteorol. Soc.*, 1996, vol. 77, pp. 437–471.
37. Gaffen, D.J., Rosen, R.D., Salstein, D.A., and Boyle, J.S., Evaluation of Tropospheric Water Vapor Simulations from the Atmospheric Intercomparison Project, *J. Climate*, 1997, vol. 10, pp. 1648–1661.
38. Doutriaux-Boucher, M., *La couverture nuageuse globale: comparaison d'observations validation de modeles de circulation generale et simulation de nouvelles technologies d'observations*, Paris: These de doctorat Universite Pierre et Marie Curie Paris, 1997.
39. Chen, C.-T. and Roeckner, E., Validation of the Earth Radiation Budget as Simulated by the Max Planck Institute for Meteorology General Circulation Model ECHAM4 Using Satellite Observations of the Earth Radiation Budget Experiment, *J. Geophys. Res.*, 1996, vol. 101, pp. 4269–4287.
40. Ramanathan, V., The Role of Earth Radiation Budget Studies in Climate and General Circulation Research, *J. Geophys. Res.*, 1987, vol. 92, pp. 4075–4095.
41. Ramanathan, V., Cess, R.D., Harrison, E.F., Minnis, P., Barkstrom, B.R., Ahmad, A., and Hartmann, D., Cloud–Radiative Forcing and Climate: Results from the Earth Radiation Budget Experiment, *Science*, 1989, vol. 243, pp. 57–63.
42. Cess, R.D., Harrison, E.F., Minnis, P., Barkstrom, B.R., Ramanathan, V., and Kwon, T.Y., Interpretation of Seasonal Cloud–Radiative Interactions Using Earth Radiation Budget Experiment Data, *J. Geophys. Res.*, 1992, vol. 97, pp. 7613–7617.
43. Li, Z.-X. and Le Treut, H., Cloud–Radiation Feedbacks in a General Circulation Model and Their Dependence on Cloud Modeling Assumptions, *Clim. Dyn.*, 1992, vol. 7, pp. 133–139.
44. Zhang, M.H., Hack, J.J., Kiehl, J.T., and Cess, R.D., Diagnostic Study of Climate Feedback Processes in Atmospheric General Circulation Model, *J. Geophys. Res.*, 1994, vol. 99, pp. 5525–5537.
45. Schlesinger, M.E. and Mitchell, J.F.B., Climate Model Simulations of Equilibrium Climatic Response to Increased Carbon Dioxide, *Rev. Geophys.*, 1987, vol. 25, pp. 137–144.
46. Cunnington, W.M. and Mitchell, J.F.B., On Dependence of Climate Sensitivity on Convection Parameterization, *Clim. Dyn.*, 1990, vol. 4, pp. 39–85.
47. Meleshko, V.P., Kattsov, V.M., Sporyshev, P.V., Vavulin, S.V., and Govorkova, V.A., Feedbacks in the Climate System: Clouds Water Vapor and Radiation Interaction, *Russ. Meteorol. Hydrol.*, 2000, vol. 2, pp. 22–45.
48. Gleckler, P.J., Randall, D.A., Boer, G., Colman, R., Dix, M., Galin, V., Helfand, M., Kiehl, J., Kitoh, A., Lau, W., Liang, X.-Z., Lykossov, V., McAvaney, B., Miyakoda, K., Planton, S., and Stern, W., Cloud–Radiative Effects on Implied Oceanic Energy Transports as Simulated by Atmospheric General Circulation Models, *Geophys. Res. Lett.*, 1995, vol. 22, pp. 791–794.
49. Covey, C., Abe-Ouchi, A., Boer, G.J., Boville, B.A., Cubasch, U., Fairhead, L., Flato, G.M., Gordon, H., Guilyardi, E., Jiang, X., Johns, T.C., Le Treut, H., Madec, G., Meehl, G.A., Miller, R., Noda, A., Power, S.B., Roeckner, E., Russell, G., Schneider, E.K., Stouffer, R.J., Terray, L., and von Storch, J.-S., The Seasonal Cycle in Coupled Ocean Atmosphere General Circulation Models, *Clim. Dyn.*, 2000, vol. 16, no. 10/11, pp. 775–787.